PERGAMON

International Journal of Solids and Structures 37 (2000) 3153–3175

INTERNATIONAL JOURNAL OF SOLIDS and STRUCTURES

www.elsevier.com/locate/ijsolstr

Three-dimensional asymptotic approach to inhomogeneous and laminated piezoelectric plates

Zhen-Qiang Cheng[a, 1], C.W. Lim[b], S. Kitipornchai[b,*]

[a]*Department of Modern Mechanics, University of Science and Technology of China, Hefei, Anhui 230026, People's Republic of China*
[b]*Department of Civil Engineering, The University of Queensland, Brisbane, Qld. 4072, Australia*

Received 13 December 1997

Abstract

An asymptotic theory is developed for anisotropic inhomogeneous and laminated piezoelectric plates on the basis of three-dimensional linear piezoelectricity. The inhomogeneity is assumed in the thickness direction and includes the important piezoelectric laminates as a special case. Through asymptotic expansions, the resulting two-dimensional differential equations are of the same form for each order, with different nonhomogeneous terms being determined systematically by preceding-order solutions. The governing equations of the leading-order, when degenerated to pure elasticity, are shown to be the same as those for equivalent classical thin elastic plates. The proposed methodology is illustrated by considering a rectangular piezoelectric plate subject to both mechanical and electric loadings with its edges simply supported and grounded. A three-dimensional solution for the fully electromechanically coupled problem is obtained by successively solving the two-dimensional field equations from the leading order to higher orders. Excellent agreement is observed with established results and new results are presented, from which significant physical insights are discussed.

Keywords: Asymptotic; Piezoelectric; Laminated plate; Non-homogeneous media; Bending

1. Introduction

Since the discovery of the piezoelectric effect by Curie brothers in 1880, research on piezoelectricity has received much attention (e.g. Tiersten, 1969; Mason, 1981; Maugin, 1988). The use of piezoelectric materials as media to transform electric and acoustic waves has made telecommunication possible.

* Corresponding author. Fax: +00-61-7-3365-3074.
E-mail address: s.kitipornchai@mailbox.uq.edu.au (S. Kitipornchai).
[1] Visiting Fellow, Department of Civil Engineering, The University of Queensland, Brisbane, Qld. 4072, Australia

0020-7683/00/$ - see front matter
PII: S0020-7683(99)00036-0

Advanced micro-electro-mechanical systems (MEMS) use piezoelectric materials in the latest technologies of smart/intelligent designs featuring miniaturization. One example is the application of the piezoelectric accelerometer to trigger an airbag in tens of thousandths of a second during an accident. The electromechanical coupling of piezoelectric materials has immense technological potential in designing smart/intelligent materials and structures ranging from huge aerospace structures to miniature medical apparatus. Because of their relative small size and light weight, piezoelectric elements can be integrated in a complex actuator network such as in robotics design without significantly affecting the structural properties of the entire system.

The development of research in piezoelectricity in the last decade has been particularly intensive. The distinctive coupling of electricity and elasticity has been foreseen to have valuable potential in engineering applications. The use of piezoelectric actuators as elements of intelligent structures was investigated by Crawley and de Luis (1987) via experiments and analytic models. Other relevant work includes those of Lee and Moon (1989), Lee (1990), Wang and Rogers (1991), Zhou and Tiersten (1994), Koconis et al. (1994a, 1994b), and Batra et al. (1996a, 1996b). A theory was proposed by Tzou (1993) and Tzou and Bao (1995) for vibration control of laminated thin shells with piezoelectric sensors and actuators. In another attempt, Mitchell and Reddy (1995) developed a hybrid laminated plate model combining the higher-order laminated plate theory for mechanical displacements and the layerwise theory for an electric potential. Reddy (1999) further extended an equivalent single-layer plate model and presented Navier solutions for rectangular laminates with integrated sensors and actuators and displacement finite element models. The possibility of tailoring adaptive materials to control vibration of aircraft wings was explored by Librescu et al. (1993, 1996, 1997). Other piezoelectric plate analyses include the work of Mindlin (1972), Tauchert (1992), and Huang and Wu (1996) in which the mechanical displacement components were modeled by either the classical or the first-order shear deformation plate theory.

To date, most two-dimensional plate models are based on either the classical Kirchhoff hypothesis or shear deformation theories which do not account for the interfacial continuity conditions. Moreover, some of the theories presume that the inplane electric field components are negligibly small compared with the transverse electric field component. However, it was revealed from the exact three-dimensional analyses of Bisegna and Maceri (1996a) and Cheng et al. (1999) that this is not always the case. On the contrary, the inplane electric field components are more significant than the transverse component in the circumstances where the electric displacements on the top and bottom surfaces of a plate are unequal.

In the light of these deficiencies in existing two-dimensional laminated piezoelectric plate models, various three-dimensional approaches have been proposed. A transfer matrix approach was developed by Sosa (1992) to study the electromechanical coupling characteristics of infinite laminated piezoelectric plates. Using modified approaches, Xu et al. (1995, 1997) and Lee and Jiang (1996) developed an analytic three-dimensional methodology for multilayered piezoelectric plates to investigate the effects of electroelastic response and obtained exact three-dimensional solutions. By extending the work of Pagano (1969, 1970) for pure elastic laminates, Heyliger (1994, 1997) and Heyliger and Brooks (1996) presented some exact solutions for laminated piezoelectric plates. All of these approaches appear to apply only to simply supported plates.

Based on the three-dimensional linear theory of piezoelectricity, a consistent theory for thin single-layer piezoelectric plates made of crystals of Class mm6 symmetry was proposed by Maugin and Attou (1990) and Bisegna and Maceri (1996b) from asymptotic approaches. A leading-order approximation of the asymptotic expansion has been given in the two studies. As stated by Maugin and Attou (1990), however, the computation of higher-order expansions requires the knowledge of the relevant boundary conditions, which could be obtained by studying the boundary layer effects along the contour of the plate. As a matter of fact, this is a difficult problem (Gol'denveizer, 1969). In general, specifying the edge boundary conditions in the sense of the Kirchhoff plate theory only yields the accurate leading-

order interior solution. The leading-order solution does not account for the through-thickness distribution of the edge boundary conditions and can not be valid near to the edges. An accurate and consistent description of the boundary conditions for solving high-order interior solutions should account for the specified edge distribution to achieve a decaying state, i.e. asymptotic to the exact solution away from edges. The modified boundary conditions differ from those for the classical Kirchhoff theory by a number of corrective terms reflecting the boundary layer effects on the interior solution.

In a recent paper, Wang and Tarn (1994) developed an asymptotic solution for bending and stretching modes of anisotropic inhomogeneous and laminated plates under lateral tractions and edge loads, where no boundary layer effects are present. Similar approaches were further extended to some other problems of simply supported plates and shells (Tarn, 1994, 1996a, 1996b; Tarn and Wang, 1994, 1995, 1997; Tarn and Yen, 1995; Wu et al., 1996a, 1996b, 1996c). The asymptotic theories developed are based on three-dimensional elasticity, and the resulting field equations of each order are reduced to two-dimensional plate and shell equations which can be successively solved to obtain an interior solution.

The asymptotic approach of Wang and Tarn (1994) in elasticity is generalized to the scope of piezoelectricity in this paper. An anisotropic inhomogeneous and laminated rectangular piezoelectric plate with its edges simply supported is considered in illustrative examples. An asymptotic three-dimensional solution for the plate is obtained and the effects of electromechanical coupling are analyzed. Excellent agreement is demonstrated with established results for laminated piezoelectric plates.

2. Formulation

Consider a plate of uniform thickness h of inhomogenous piezoelectric materials. Let a Cartesian coordinate system $\{x_i\}$ ($i = 1,2,3$) be used such that the bottom and top surfaces of the undeformed plate lie in the planes $x_3 = 0$ and h, with the reference plane being $x_3 = 0$. Throughout this paper, the Einsteinian summation convention applies, unless otherwise specified, to repeated indices of tensor components, with Latin indices ranging from 1 to 3 while Greek indices over 1 and 2. The dependence of functions and operators on x_α and x_3 is not shown explicitly unless necessary.

The description of linear piezoelectricity is based on the elements of elasticity, electrodynamics and their coupled interactions by means of two mechanical variables, the stress and strain tensors τ_{ij} and S_{kl}, and two electric variables, the electric displacement and electric field vectors D_i and E_k. In the absence of body forces and electric charge density, the field equations of elastic equilibrium and Gauss' law of electrostatics are (Tiersten, 1969; Maugin, 1988)

$$\tau_{ij,j} = 0, \quad D_{i,i} = 0. \tag{1}$$

The strain and electric field are related to the elastic displacements u_k and the electric potential φ through the gradient relations:

$$S_{kl} = \frac{1}{2}(u_{k,l} + u_{l,k}), \qquad E_k = -\varphi_{,k}, \tag{2}$$

where the second equation implies a quasi-static approximation.

Since there are only 13 relations in the above equations for 22 unknowns, the following 9 additional equations for constitutive relations are complemented for a complete formulation of the linear theory of static piezoelectricity

$$\tau_{ij} = c_{ijkl}S_{kl} - e_{kij}E_k,$$

$$D_i = e_{ikl}S_{kl} + \varepsilon_{ik}E_k, \tag{3}$$

where c_{ijkl} is the fourth-order elastic tensor measured at a constant electric field, e_{kij} the third-order piezoelectric tensor, and ε_{ik} the second-order dielectric tensor measured at a constant strain. These material moduli exhibit the following symmetries

$$c_{ijkl} = c_{jikl} = c_{klij},$$

$$e_{kij} = e_{kji},$$

$$\varepsilon_{ik} = \varepsilon_{ki}. \tag{4}$$

In particular, the constitutive relations for a monoclinic piezoelectric material with a binary axis parallel to the x_3-axis can be cast as

$$\tau_{\alpha\beta} = c_{\alpha\beta\omega\rho}S_{\omega\rho} + c_{\alpha\beta33}S_{33} - e_{3\alpha\beta}E_3, \tag{5a}$$

$$\tau_{\alpha3} = 2c_{\alpha3\omega3}S_{\omega3} - e_{\omega\alpha3}E_\omega, \tag{5b}$$

$$\tau_{33} = c_{33\omega\rho}S_{\omega\rho} + c_{3333}S_{33} - e_{333}E_3, \tag{5c}$$

$$D_\alpha = 2e_{\alpha\omega3}S_{\omega3} + \varepsilon_{\alpha\omega}E_\omega \tag{5d}$$

and

$$D_3 = e_{3\omega\rho}S_{\omega\rho} + e_{333}S_{33} + \varepsilon_{33}E_3, \tag{5e}$$

or, in matrix form,

$$\begin{bmatrix} \tau_{11} \\ \tau_{22} \\ \tau_{33} \\ \tau_{23} \\ \tau_{31} \\ \tau_{12} \\ D_1 \\ D_2 \\ D_3 \end{bmatrix} = \begin{bmatrix} c_{1111} & c_{1122} & c_{1133} & 0 & 0 & c_{1112} & 0 & 0 & e_{311} \\ & c_{2222} & c_{2233} & 0 & 0 & c_{2212} & 0 & 0 & e_{322} \\ & & c_{3333} & 0 & 0 & c_{3312} & 0 & 0 & e_{333} \\ & & & c_{2323} & c_{2313} & 0 & e_{123} & e_{223} & 0 \\ & & & & c_{1313} & 0 & e_{113} & e_{213} & 0 \\ & & & & & c_{1212} & 0 & 0 & e_{312} \\ & & \text{sym.} & & & & -\varepsilon_{11} & -\varepsilon_{12} & 0 \\ & & & & & & & -\varepsilon_{22} & 0 \\ & & & & & & & & -\varepsilon_{33} \end{bmatrix} \begin{bmatrix} S_{11} \\ S_{22} \\ S_{33} \\ 2S_{23} \\ 2S_{31} \\ 2S_{12} \\ -E_1 \\ -E_2 \\ -E_3 \end{bmatrix}. \tag{6}$$

Here, the only material symmetry is assumed to be of reflectional symmetry in planes parallel to the surfaces of the plate. Accordingly, the numbers of independent elastic, piezoelectric and dielectric moduli are, respectively, 13, 8 and 4 for the monoclinic materials. The inhomogeneity of materials is with respect to x_3 only, i.e.

$$c_{ijkl} \equiv c_{ijkl}(x_3),$$

$$e_{kij} \equiv e_{kij}(x_3),$$

$$\varepsilon_{ik} \equiv \varepsilon_{ik}(x_3). \tag{7}$$

In particular, if the plate is a layered or laminated medium, comprised of layers of different homogeneous monoclinic piezoelectric materials, then the material moduli are piecewise constant functions of x_3.

Eqs. (1), (2), (5c) and (5e) may be reformulated as

$$u_{\omega,3} = -u_{3,\omega} + 2S_{\omega 3},$$

$$\tau_{33,3} = -\tau_{\alpha 3,\alpha},$$

$$D_{3,3} = -D_{\rho,\rho},$$

$$\tau_{\alpha 3,3} = -\tau_{\alpha\beta,\beta},$$

$$c_{333}u_{3,3} + e_{333}\varphi_{,3} = \tau_{33} - c_{33\omega\rho}S_{\omega\rho} \text{ and}$$

$$e_{333}u_{3,3} - \varepsilon_{33}\varphi_{,3} = D_3 - e_{3\omega\rho}S_{\omega\rho}. \tag{8}$$

By substituting Eqs. (5a) and (5d) into Eq. (8) to eliminate $\tau_{\alpha\beta}$ and D_ρ, and expressing $S_{\omega 3}$ from Eq. (5b) in terms of $\tau_{\alpha 3}$ and φ, the following transfer matrix equation can be given

$$\partial_z \begin{bmatrix} \mathbf{F} \\ \mathbf{G} \end{bmatrix} = \varepsilon \begin{bmatrix} \mathbf{0} & \mathbf{A} \\ \mathbf{B} & \mathbf{0} \end{bmatrix} \begin{bmatrix} \mathbf{F} \\ \mathbf{G} \end{bmatrix}, \tag{9}$$

where we have scaled the thickness coordinate $x_3 = \varepsilon z$, and thus $\varepsilon\partial/\partial x_3 = \partial/\partial z \equiv \partial_z$, from the range of $x_3 \in [0,h]$ to the range of $z \in [0,a]$ by a small thickness parameter $\varepsilon = h/a$, with a being a typical inplane dimension. The field functions are chosen as

$$\mathbf{F} = \begin{bmatrix} u_1 \\ u_2 \\ \tau_{33} \\ D_3 \end{bmatrix},$$

$$\mathbf{G} = \begin{bmatrix} \tau_{13} \\ \tau_{23} \\ u_3 \\ \varphi \end{bmatrix}, \tag{10}$$

which ensure the continuity condition of the relevant physical quantities across each layer interface according to the requirements of equilibrium and material continuity. The 4×4 operator matrices, $\mathbf{A}$ and $\mathbf{B}$, contain the inplane differential operator $\partial_\alpha \equiv \partial/\partial x_\alpha$ and depend on z only through the material moduli:

$$\mathbf{A} = \begin{bmatrix} \mathbf{I} & -\mathbf{J}_\beta\partial_\beta \\ -\mathbf{J}_\beta^T\partial_\beta & \mathbf{K}_{\beta\rho}\partial_\beta\partial_\rho \end{bmatrix},$$

$$\mathbf{B} = \begin{bmatrix} -\mathbf{L}_{\beta\rho}\partial_\beta\partial_\rho & -\mathbf{M}_\beta\partial_\beta \\ -\mathbf{M}_\beta^T\partial_\beta & \mathbf{N} \end{bmatrix}, \tag{11}$$

where $\mathbf{A}$ and $\mathbf{B}$ have been partitioned into 2×2 operator sub-matrices. $\mathbf{I}$ and $\mathbf{N}$ are the matrices with each of their elements being a scalar defined by

$$\mathbf{I} = (I^{\omega\alpha}) = \left(c^{-1}_{\omega 3\alpha 3}\right) = \frac{1}{c_{1313}c_{2323} - c_{1323}^2}\begin{bmatrix} c_{2323} & -c_{1323} \\ -c_{1323} & c_{1313} \end{bmatrix}, \text{ or}$$

or

$$(c_{3\alpha\omega 3}) = \begin{bmatrix} c_{1313} & c_{1323} \\ c_{1323} & c_{2323} \end{bmatrix},$$

$$\mathbf{N} = (N^{\alpha\omega}) = \frac{1}{c_{3333}\varepsilon_{33} + e_{333}^2}\begin{bmatrix} \varepsilon_{33} & e_{333} \\ e_{333} & -c_{3333} \end{bmatrix}, \text{ or}$$

or

$$\mathbf{N}^{-1} = \begin{bmatrix} c_{3333} & e_{333} \\ e_{333} & -\varepsilon_{33} \end{bmatrix}. \tag{12}$$

Denoting $\delta_{\omega\beta}$ as the Kronecker delta function, $\mathbf{J}_\beta$ and $\mathbf{M}_\beta$ are the matrices with each of their elements being a vector defined by

$$\begin{bmatrix} J_\beta^{\omega 1} & J_\beta^{\omega 2} \end{bmatrix} = \begin{bmatrix} \delta_{\omega\beta} & I^{\omega\alpha}e_{\beta\alpha 3} \end{bmatrix},$$

$$\begin{bmatrix} M_\beta^{\alpha 1} & M_\beta^{\alpha 2} \end{bmatrix} = [c_{\alpha\beta 33} \quad e_{3\alpha\beta}]\mathbf{N}, \tag{13}$$

and $\mathbf{K}_{\beta\rho}$ and $\mathbf{L}_{\beta\rho}$ are the matrices with each of their elements being a tensor defined by

$$K_{\beta\rho}^{11} = K_{\beta\rho}^{12} = K_{\beta\rho}^{21} = 0,$$

$$K_{\beta\rho}^{22} = J_\beta^{\omega 2}e_{\rho\omega 3} + \varepsilon_{\beta\rho},$$

$$L_{\beta\rho}^{\alpha\omega} = c_{\alpha\beta\omega\rho} - M_\beta^{\alpha 1}c_{33\omega\rho} - M_\beta^{\alpha 2}e_{3\omega\rho}. \tag{14}$$

Here, we have used the superscripts, to which the conventional summation also applies, to denote the row and column indices of a matrix element in order to distinguish the subscripts of the corresponding element which is a vector or a tensor. These sub-matrices are only related to the material moduli depending on x_3. The inplane stresses and inplane electric displacements, which may be discontinuous in x_3, are given by

$$\tau_{\alpha\beta} = L_{\beta\rho}^{\alpha\omega}\partial_\rho u_\omega + M_\beta^{\alpha 1}\tau_{33} + M_\beta^{\alpha 2}D_3, \text{ and}$$

and

$$D_\rho = J_\rho^{\alpha 2}\tau_{\alpha 3} - K_{\beta\rho}^{22}\partial_\beta\varphi. \tag{15}$$

3. An asymptotic approach

The general problem of piezoelectricity is to determinate the global and local electroelastic field under applied mechanical and electric loadings. In this paper, the mechanical loading is specified by the shear tractions $q_\alpha^\pm$ and the normal tractions $q_3^\pm$ imposed on the plate surfaces. Assume that the two surfaces of the plate are coated with very thin conducting electrodes which may carry an alternating forcing potential. For simplicity, the thickness of each electrode is considered to be negligibly small, giving a mathematical surface with a specified electric potential. Specifically, the electric load is given by applied potentials $V^\pm$. A short circuit condition corresponds to the same electric potentials holding on the electroded surfaces.

For general mechanical loading conditions (in particular, the tractions on the top and bottom surfaces are not equal), the shear stresses are of the order $O(\varepsilon^2)$ and the normal stress is of the order $O(\varepsilon^3)$, as in the case of pure elasticity (Wang and Tarn, 1994). These surface forcing functions are then scaled as

$$\tau_{\alpha 3}(x_\rho,0) = \varepsilon^2 q_\alpha^-(x_\rho), \tag{16a}$$

$$\tau_{\alpha 3}(x_\rho,a) = \varepsilon^2 q_\alpha^+(x_\rho), \tag{16b}$$

$$\tau_{33}(x_\rho,0) = -\varepsilon^3 q_3^-(x_\rho), \tag{17a}$$

$$\tau_{33}(x_\rho,a) = -\varepsilon^3 q_3^+(x_\rho). \tag{17b}$$

The surface electric potentials are constructed to be of the order $O(\varepsilon^2)$, i.e.

$$\varphi(x_\rho,0) = \varepsilon^2 V^-(x_\rho), \tag{18a}$$

$$\varphi(x_\rho,a) = \varepsilon^2 V^+(x_\rho). \tag{18b}$$

To find solutions of successive approximations, we express the field functions $\mathbf{F}$ and $\mathbf{G}$ in the form of regular expansion in terms of the small thickness parameter ε as

$$\begin{bmatrix} \mathbf{F} \\ \mathbf{G} \end{bmatrix} = \sum_{n=0}^{\infty} \varepsilon^{2n} \begin{bmatrix} \varepsilon \mathbf{f}^{(n)} \\ \mathbf{g}^{(n)} \end{bmatrix}. \tag{19}$$

Note that the above expansion terms only contain odd powers of the small parameter ε for $\mathbf{F}$ and even powers for $\mathbf{G}$. This is because all of the complemented expansion terms, even powers for $\mathbf{F}$ and odd powers for $\mathbf{G}$, will result in homogeneous equations and thus furnish a trivial solution. All of the inhomogeneous parts contributed by the mechanical and electric loads as scaled by Eqs. (16)–(18) can be accounted for by only using Eq. (19). Specifically, the surface traction conditions (Eqs. (16) and (17)) and the surface electric potential conditions (18) may be expressed by the components of the expansion in Eq. (19) for $\mathbf{F}$ and $\mathbf{G}$ as, for the leading order,

$$g_\alpha^{(0)}(0) = \tau_{\alpha 3}^{(0)}(0) = 0,$$

$$g_\alpha^{(0)}(a) = \tau_{\alpha 3}^{(0)}(a) = 0,$$

$$f_3^{(0)}(0) = \tau_{33}^{(0)}(0) = 0,$$

$$f_3^{(0)}(a) = \tau_{33}^{(0)}(a) = 0,$$

$$g_4^{(0)}(0) = \varphi^{(0)}(0) = 0,$$

$$g_4^{(0)}(a) = \varphi^{(0)}(a) = 0, \tag{20}$$

and, for the remaining orders,

$$g_\alpha^{(n+1)}(0) = \tau_{\alpha 3}^{(n+1)}(0) = q_\alpha^- \delta_{n0},$$

$$g_\alpha^{(n+1)}(a) = \tau_{\alpha 3}^{(n+1)}(a) = q_\alpha^+ \delta_{n0},$$

$$f_3^{(n+1)}(0) = \tau_{33}^{(n+1)}(0) = -q_3^- \delta_{n0},$$

$$f_3^{(n+1)}(a) = \tau_{33}^{(n+1)}(a) = -q_3^+ \delta_{n0},$$

$$g_4^{(n+1)}(0) = \varphi^{(n+1)}(0) = V^- \delta_{n0},$$

$$g_4^{(n+1)}(a) = \varphi^{(n+1)}(a) = V^+ \delta_{n0}, \ (n \geq 0). \tag{21}$$

Substituting the expansion in Eq. (19) into Eq. (9) leads to the simple recurrence relations as

$$\partial_z \mathbf{g}^{(0)} = \mathbf{0},$$

$$\partial_z \mathbf{f}^{(n)} = \mathbf{A}\mathbf{g}^{(n)},$$

$$\partial_z \mathbf{g}^{(n+1)} = \mathbf{B}\mathbf{f}^{(n)}, \ (n \geq 0). \tag{22}$$

The resulting recurrence relations suggest that a solution can be obtained by successively integrating these differential equations with respect to z and using Eqs. (20) and (21) for the bottom surface

$$\mathbf{g}^{(0)} = \begin{bmatrix} 0 \\ 0 \\ U_3^{(0)} \\ 0 \end{bmatrix}, \tag{23a}$$

$$\mathbf{f}^{(n)} = \begin{bmatrix} U_1^{(n)} \\ U_2^{(n)} \\ -q_3^- \delta_{n1} \\ D_0^{(n)} \end{bmatrix} + Q\mathbf{A}\mathbf{g}^{(n)}, \tag{23b}$$

$$\mathbf{g}^{(n+1)} = \begin{bmatrix} q_1^- \delta_{n0} \\ q_2^- \delta_{n0} \\ U_3^{(n+1)} \\ V^- \delta_{n0} \end{bmatrix} + Q\mathbf{B}\mathbf{f}^{(n)}, \ (n \geq 0), \tag{23c}$$

where the fundamental unknowns are some of the components of the expanded field functions, i.e. the components of three mechanical displacements and the electric displacement at the bottom surface $z = 0$ of the plate,

$$U_\omega^{(n)} \equiv u_\omega^{(n)}(x_\rho, 0),$$

$$U_3^{(n)} \equiv u_3^{(n)}(x_\rho, 0),$$

$$D_0^{(n)} \equiv D_3^{(n)}(x_\rho, 0^+), \tag{24}$$

with the integral operator being

$$Q(\cdots) \equiv \int_0^z (\cdots) \mathrm{d}z. \tag{25}$$

Most plate theories implicitly designate the midplane of a plate to be the reference plane and hence the fundamental unknowns are those at the midplane. It is clear, however, that at least four components of the unknown functions **F** and **G** will be known *a priori* when we choose either of the plate surfaces to be the reference plane. Accordingly, the problem will be reduced to determining the remaining components of the unknown functions. For the specific problem in which the surface tractions and the surface electric potentials are prescribed by Eqs. (16)–(18), the fundamental unknowns have been chosen as the physical quantities on the bottom surface of the plate, i.e. Eq. (24). These unknowns have to be determined in such a way that the conditions (Eqs. (16)–(18)) for the tractions and the electric potential on the top surface $z = a$ are satisfied through Eqs. (23a), (23b) and (23c).

Substituting the expression of $\mathbf{g}^{(n)}$ from Eq. (23c) into Eq. (23b) results in an alternative expression

$$\mathbf{f}^{(n)} = \mathbf{X}^{(n)} + \mathbf{H}^{(n)}, \tag{26}$$

where

$$\mathbf{X}^{(n)} = \begin{bmatrix} U_1^{(n)} - z\partial_1 U_3^{(n)} \\ U_2^{(n)} - z\partial_2 U_3^{(n)} \\ 0 \\ D_0^{(n)} \end{bmatrix}, \tag{27a}$$

$$\mathbf{H}^{(n)} = \delta_{n1} \left\{ Q\mathbf{A} \begin{bmatrix} q_1^- \\ q_2^- \\ 0 \\ V^- \end{bmatrix} - \begin{bmatrix} 0 \\ 0 \\ q_3^- \\ 0 \end{bmatrix} \right\} + Q\mathbf{A}Q\mathbf{B}\mathbf{f}^{(n-1)}. \tag{27b}$$

With Eqs. (26) and (27b), the auxiliary function $\mathbf{H}^{(n)}$ are found to have the following recurrence relation

$$\mathbf{H}^{(n+1)} = \delta_{n0}\left\{ Q\mathbf{A}\begin{bmatrix} q_1^- \\ q_2^- \\ 0 \\ V^- \end{bmatrix} - \begin{bmatrix} 0 \\ 0 \\ q_3^- \\ 0 \end{bmatrix}\right\} + Q\mathbf{A}Q\mathbf{B}(\mathbf{X}^{(n)} + \mathbf{H}^{(n)}), \tag{28}$$

with the leading term $\mathbf{H}^{(0)} = \mathbf{0}$.

By denoting the integral operators

$$\bar{Q}(\cdots) \equiv \int_0^a (\cdots)\mathrm{d}z, \tag{29}$$

the traction and the electric potential conditions (21) on the top surface of the plate can be recast, through Eqs. (23a), (23b) and (23c), as

$$\bar{Q}B_{\alpha L} f_L^{(n)} = \left(q_\alpha^+ - q_\alpha^-\right)\delta_{n0}, \tag{30a}$$

$$\bar{Q}A_{3L} g_L^{(n+1)} = -\left(q_3^+ - q_3^-\right)\delta_{n0} \tag{30b}$$

and

$$\bar{Q}B_{4L} f_L^{(n)} = (V^+ - V^-)\delta_{n0}, \tag{30c}$$

where an upper case subscript L takes the values from 1 to 4 and the implicit summation convention also applies. Further, using Eq. (23c) and noting that $A_{3\alpha} = -\partial_\alpha$ and $A_{33} = A_{34} = 0$, Eq. (30b) can be rewritten as

$$-\bar{Q}(a-z)B_{\alpha L}\partial_\alpha f_L^{(n)} = \left[-\left(q_3^+ - q_3^-\right) + a\partial_\alpha q_\alpha^-\right]\delta_{n0}, \tag{31}$$

which, when taken with Eq. (30a), gives

$$\bar{Q}zB_{\alpha L}\partial_\alpha f_L^{(n)} = \left[-\left(q_3^+ - q_3^-\right) + a\partial_\alpha q_\alpha^+\right]\delta_{n0}. \tag{32}$$

Eqs. (30a), (32) and (30c) can be recast, with the aid of Eq. (26), in the form of the matrix equation

$$\mathbf{R}(\mathbf{X}^{(n)} + \mathbf{H}^{(n)}) = \delta_{n0}\mathbf{Y}, \tag{33}$$

or, denoting $\mathbf{R}\mathbf{X}^{(n)} \equiv \tilde{\mathbf{R}}\tilde{\mathbf{X}}^{(n)}$,

$$\tilde{\mathbf{R}}\tilde{\mathbf{X}}^{(n)} = \delta_{n0}\mathbf{Y} - \mathbf{R}\mathbf{H}^{(n)}, \tag{34}$$

where

$$\tilde{\mathbf{X}}^{(n)} = \begin{bmatrix} U_1^{(n)} & U_2^{(n)} & U_3^{(n)} & D_0^{(n)} \end{bmatrix}^T. \tag{35}$$

The components of the operator matrices $\tilde{\mathbf{R}}$ and $\mathbf{R}$ are expressed as

$$\tilde{R}_{\alpha\omega} = R_{\alpha\omega} = -\bar{Q}L_{\beta\rho}^{\alpha\omega}\partial_\beta\partial_\rho,$$

$$\tilde{R}_{\alpha 3} = \bar{Q}zL_{\beta\rho}^{\alpha\omega}\partial_\beta\partial_\omega\partial_\rho,$$

$$R_{\alpha 3} = -\bar{Q} M_{\beta}^{\alpha 1} \partial_{\beta},$$

$$\tilde{R}_{\alpha 4} = R_{\alpha 4} = -\bar{Q} M_{\beta}^{\alpha 2} \partial_{\beta},$$

$$\tilde{R}_{3\omega} = R_{3\omega} = -\bar{Q} z L_{\beta\rho}^{\alpha\omega} \partial_{\alpha} \partial_{\beta} \partial_{\rho},$$

$$\tilde{R}_{33} = \bar{Q} z^2 L_{\beta\rho}^{\alpha\omega} \partial_{\alpha} \partial_{\beta} \partial_{\omega} \partial_{\rho},$$

$$R_{33} = -\bar{Q} z M_{\beta}^{\alpha 1} \partial_{\alpha} \partial_{\beta},$$

$$\tilde{R}_{34} = R_{34} = -\bar{Q} z M_{\beta}^{\alpha 2} \partial_{\alpha} \partial_{\beta},$$

$$\tilde{R}_{4\omega} = R_{4\omega} = -\bar{Q} M_{\beta}^{\omega 2} \partial_{\beta},$$

$$\tilde{R}_{43} = \bar{Q} z M_{\beta}^{\omega 2} \partial_{\beta} \partial_{\omega},$$

$$R_{43} = \bar{Q} N^{21},$$

$$\tilde{R}_{44} = R_{44} = \bar{Q} N^{22} \tag{36}$$

and the components of $\mathbf{Y}$ involved in the effective loads on the right hand side of Eq. (34) are

$$Y_{\alpha} = q_{\alpha}^{+} - q_{\alpha}^{-},$$

$$Y_3 = -\left(q_3^{+} - q_3^{-}\right) + a \partial_{\alpha} q_{\alpha}^{+}$$

and

$$Y_4 = V^{+} - V^{-}. \tag{37}$$

Eq. (34) gives the crucial field equations obtained through the field asymptotic approach, from which the unknowns Eq. (35) of each order can be solved with specified edge conditions at the reference plane for any set of given material parameters and load parameters. It is obvious from Eq. (34) that $\mathbf{Y}$ is only related to the field equation at the leading-order ($n = 0$), while $\mathbf{H}^{(n)}$ only contributes to the higher-order field equations due to $\mathbf{H}^{(0)} = \mathbf{0}$. Since $\mathbf{Y}$ is known *a priori* from Eq. (37), the unknowns of the leading order can be determined from the field equation of the leading order. Then $\mathbf{H}^{(1)}$ can be obtained from Eq. (28) and, hence, the unknowns for $n = 1$ can be solved from the associated boundary value problem of the corresponding order. Such a procedure may be continued in this way to higher orders, giving a simple recurrence process. The higher-order solutions may be considered as the corrections to the leading-order solution. Therefore, it shows how a full three-dimensional interior solution can be obtained to any desired degree of accuracy.

The differential operator, $\tilde{\mathbf{R}}$, as given by Eq. (36) for the field equations (34) may be recognized, if degenerated from piezoelectricity to pure elasticity, as being identical with that of the classical plate

theory (Whitney, 1987; Reddy, 1997) for the bending of a thin monoclinic plate or laminate. Moreover, the matrix operators $\tilde{\mathbf{R}}$ and $\mathbf{R}$ involved in Eq. (34) have the same form for the field equations of all orders. Apart from $\mathbf{Y}$, which is nontrivial only for the leading order, the effective loads on the right-hand side of Eq. (34) only involves the derivatives of the auxiliary function $\mathbf{H}^{(n)}$ with respect to x_α and its integration with respect to z. The auxiliary function of higher-order may be obtained from its preceding lower-order solution according to Eq. (28), which involves those operators being the same for all orders. Consequently, any numerical technique can easily be applied to the field asymptotic equations by always solving the same equations for piezoelectric plates, with the effective loads being simply determined by lower-order solutions.

4. Illustrative example

Two different piezoelectric laminated plates made of lead zirconate titanate (PZT-4) and polyvinylidene fluoride (PVDF) are considered to illustrate the asymptotic method presented in this paper. They are a two-layer laminate of dissimilar piezoelectric materials PZT-4/PVDF and a three-layer PVDF laminate. These plates are rectangular and of equal thickness for each layer. Their edges are simply supported and grounded at $x_1=0,a$ and $x_2=0,b$, i.e.

$$u_2 = u_3 = \tau_{11} = \varphi = 0, \text{ on } x_1 = 0,a \text{ and}$$

$$u_1 = u_3 = \tau_{22} = \varphi = 0, \text{ on } x_2 = 0,b. \tag{38}$$

The mechanical and electric loadings are specified as

$$q_1^{\pm} = \hat{q}_1^{\pm} \cos l_1 x_1 \sin l_2 x_2,$$

$$q_2^{\pm} = \hat{q}_2^{\pm} \sin l_1 x_1 \cos l_2 x_2,$$

$$q_3^{\pm} = \hat{q}_3^{\pm} \sin l_1 x_1 \sin l_2 x_2 \text{ and}$$

$$V^{\pm} = \hat{V}^{\pm} \sin l_1 x_1 \sin l_2 x_2, \tag{39}$$

with

$$l_1 = \frac{m_1 \pi}{a} \text{ and}$$

$$l_2 = \frac{m_2 \pi}{b} \tag{40}$$

where a quantity with a hat denotes the amplitude of the corresponding physical quantity. The peak values (i.e. amplitude) of these quantities may not occur at the same location as there could be a phase lag. For the specific problem, the pointwise edges conditions (38) can be satisfied both mechanically and electrically by assuming

$$\tilde{\mathbf{X}}^{(n)} = \begin{bmatrix} U_1^{(n)} \\ U_2^{(n)} \\ U_3^{(n)} \\ D_0^{(n)} \end{bmatrix} = \begin{bmatrix} \hat{U}_1^{(n)} \cos l_1 x_1 \sin l_2 x_2 \\ \hat{U}_2^{(n)} \sin l_1 x_1 \cos l_2 x_2 \\ \hat{U}_3^{(n)} \sin l_1 x_1 \sin l_2 x_2 \\ \hat{D}_0^{(n)} \sin l_1 x_1 \sin l_2 x_2 \end{bmatrix}. \tag{41}$$

Solutions of each order may be conducted in the way described earlier, generating numerical results to the desired degree of accuracy for the specific problem.

The material moduli of PZT-4 (Berlincourt et al., 1964) and PVDF (Tashiro et al., 1981) are summarized in Table 1, where ε_0 is the permittivity of a vacuum. Those moduli used by Heyliger (1997) are enclosed in parentheses wherever different from the original values. Emphasis should be placed on e_{113} which is not available (marked by stars) in both papers (Heyliger and Brooks, 1996; Heyliger, 1997). It is found that $e_{113} = e_{223}$ was used by Heyliger et al. (1996). However, this relation is only valid for PZT-4 but not for PVDF because of mm2 symmetry of the PVDF material.

Throughout the following examples, two loading conditions are examined. One is termed as applied load, corresponding to normal traction q_3^+ on the top surface with vanishing electric potential, and another termed as applied potential, corresponding to electric potential V^+ on the top surface with vanishing normal traction. For both loading conditions, mechanical and electric loadings on the bottom surface and shear tractions on the top surface are set to zero, i.e. $q_3^- = V^- = q_\alpha^\pm = 0$. In addition, $m_1 = m_2 = 1$ is used.

A comparison study for a PZT-4/PVDF laminate with reference to Heyliger (1997) is presented in Table 2. This is a rectangular laminate with PZT-4 on the top and PVDF on the bottom and with equal thickness. The aspect ratio is $a/b = 2$ and the span-to-thickness ratio is $a/h = 10$. The mechanical and

Table 1
Moduli of piezoelectric materials

Moduli	PZT-4	PVDF
c_{1111} (GPa)	139	238.24 (238)
c_{2222} (GPa)	139	23.6
c_{3333} (GPa)	115	10.64 (10.6)
c_{1122} (GPa)	77.8	3.98
c_{1133} (GPa)	74.3	2.19
c_{2233} (GPa)	74.3	1.92
c_{2323} (GPa)	25.6	2.15
c_{3131} (GPa)	25.6	4.4
c_{1212} (GPa)	30.6	6.43
e_{311} (C/m^2)	−5.2	−0.13
e_{322} (C/m^2)	−5.2	−0.145 (−0.14)
e_{333} (C/m^2)	15.1 (15.08)	−0.276 (−0.28)
e_{223} (C/m^2)	12.7 (12.72)	−0.009 (−0.01)
e_{113} (C/m^2)	12.7 (****)[b]	−0.135 (****)[b]
$\varepsilon_{11}/\varepsilon_0$ [a]	1475	12.5
$\varepsilon_{22}/\varepsilon_0$ [a]	1475	11.98
$\varepsilon_{33}/\varepsilon_0$ [a]	1300	11.98

[a] $\varepsilon_0 = 8.854185$ pF/m.
[b] (****): values not available in Heyliger (1997).

electric quantities are non-dimensionalized by

$$\bar{u}_i = \frac{u_i}{Pa}, \quad \bar{\tau}_{ij} = \frac{\tau_{ij}}{Pc^*}, \quad \bar{\varphi} = \frac{e^*\varphi}{Pac^*} \quad \text{and} \quad \bar{D}_i = \frac{D_i}{Pe^*}, \tag{42}$$

where either $P = -\hat{q}q_3^+/c^*$ for applied load or $P = \hat{V}^+(e^*/ac^*)$ for applied potential, with $c^* = 1\ \mathrm{N/m^2}$ and $e^* = 1\ \mathrm{C/m^2}$. For the purpose of consistent comparison, the moduli values used by Heyliger (1997) have been adopted only to calculate the results in Table 2 and, in particular, $e_{113} = e_{223} = -0.01$ for PVDF have been employed. The order of solution is increased from 0 to 7 where the higher-order solutions are obtained via the recurrence procedure described in Section 3. It can be seen that the second-order results are quite good. Numerical convergence to four significant digits is reached for the 7th-order solutions and thus subsequent higher-order solutions are not necessary. As observed, the 7th-order solutions are in excellent agreement with the results of Heyliger (1997). The slight numerical difference in this comparison is possibly due to numerical truncation errors of PZT-4 and PVDF moduli between Heyliger (1997) and this work.

Hereafter, the original moduli of PZT-4 and PVDF in Table 1, taken from Berlincourt et al. (1964) and Tashiro et al. (1981), are used and, in particular, $e_{113} = -0.135$ is adopted. As a corrective step and for future reference, the dimensionless electric potential through the plate thickness for the above two-layer PZT-4/PVDF laminate is presented in Fig. 1 for applied load and in Fig. 2 for applied potential. As expected, the electric potentials in Figs. 1 and 2 are nonlinear through the thickness considering the entire laminate as a whole. Specifically, it is possible to assume the electric potential to be (i) a piecewise quadratic distribution for a laminate under applied load, as in Fig. 1, and (ii) a piecewise linear distribution for a laminate under applied potential, as in Fig. 2.

It has been discovered by Bisegna and Maceri (1996a) from a thin single-layer plate limit and by Cheng et al. (1999) from an exact analytic solution of laminates, thin or thick, that the assumption of neglecting inplane electric field in two-dimensional thin piezoelectric plate models is satisfactory if $D_3^+ - D_3^- = 0$. This is because the ratio of inplane electric field to the transverse electric field is of the order of plate thickness, which is a small quantity. For the cases when $D_3^+ - D_3^- \neq 0$, those thin piezoelectric plate models are unjustified as they have neglected the inplane electric field which, compared with the

Table 2
Comparison of solutions of different orders at amplitude with exact results for a two-layer PZT-4/PVDF laminate ($a/b = 2$, $a/h = 10$)

Order	Applied load			
	$\bar{u}_1\ (x_3 = 0)$	$\bar{D}_3\ (x_3 = h)$	$\bar{\tau}_{13}\ (x_3 = h/2)$	$\bar{\tau}_{33}\ (x_3 = h/2)$
0	1.524e−11	1.225e−11	0	0
1	1.397e−11	1.836e−10	1.232	0.4007
2	1.416e−11	2.044e−10	1.140	0.3513
7	1.413e−11	2.014e−10	1.150	0.3572
Heyliger (1997)	1.414e−11	2.011e−10	1.149	0.3571
	Applied potential			
0	−2.743e−12	−2.254e−9	0	0
1	−1.890e−11	−4.978e−8	−0.0836	0.0121
2	−1.602e−11	−4.734e−8	−0.4120	−0.2289
7	−1.640e−11	−4.749e−8	−0.3478	−0.1851
Heyliger (1997)	−1.640e−11	−4.752e−8	−0.3451	−0.1869

transverse electric field, is of order of the reciprocal of plate thickness. Such a significant physical insight is consistent with the numerical result given in Fig. 3.

Fig. 3 shows the amplitude ratio $\hat{E}_1/\hat{E}_3$ of the inplane-to-transverse electric field components which is discontinuous at the PZT-4/PVDF interface. It is noticed that although the inplane electric field is negligible within the PVDF layer, on the contrary, it is more significant than the transverse electric field in the PZT-4 layer, and $\hat{E}_2$ is even more pronounced as $\hat{E}_2 = 2\hat{E}_1$. Consequently, the assumption of a negligible inplane electric field is unjustifiable, at least in the present case.

Numerical results are given for a three-ply (0°/90°/0°) PVDF piezoelectric plate, with each ply being homogeneous and having equal thickness. The plate is infinitely wide ($b \to \infty$) such that $a/b \to 0$, and thus we have $u_2 = D_2 = \tau_{12} = \tau_{23} = 0$. Although a range of results has been graphically given by Heyliger and Brooks (1996), we present a wider spectrum of the physical quantities in tabulated form. There is a two-fold purpose here. The first purpose is to present more accurate results using $e_{113} = -0.135$ for PVDF as compared to the results of Heyliger and Brooks (1996) where $e_{113} = -0.01$ was used. The second purpose is to provide a complete set of results of the physical quantities as a benchmark for future references.

The asymptotic solutions for mechanical displacements, stresses, electric potential and electric displacements through the plate thickness are presented in Tables 3–11 to the accuracy as presented. Tables 3–8 contain peak values of the dimensionless quantities ($\bar{u}_1$, $\bar{u}_3$, $\bar{\tau}_{13}$, $\bar{\tau}_{33}$, $\bar{\varphi}$ and $\bar{D}_3$) continuous across the interfaces, while Tables 9–11 contain peak values of the dimensionless quantities ($\bar{\tau}_{11}$, $\bar{\tau}_{22}$ and $\bar{D}_1$) discontinuous across the interfaces. The span-to-thickness ratio, a/h, increases from 4 (a moderately thick plate) to 100 (a thin plate). The point in the thickness direction extends from $x_3 = 0$ (bottom) to

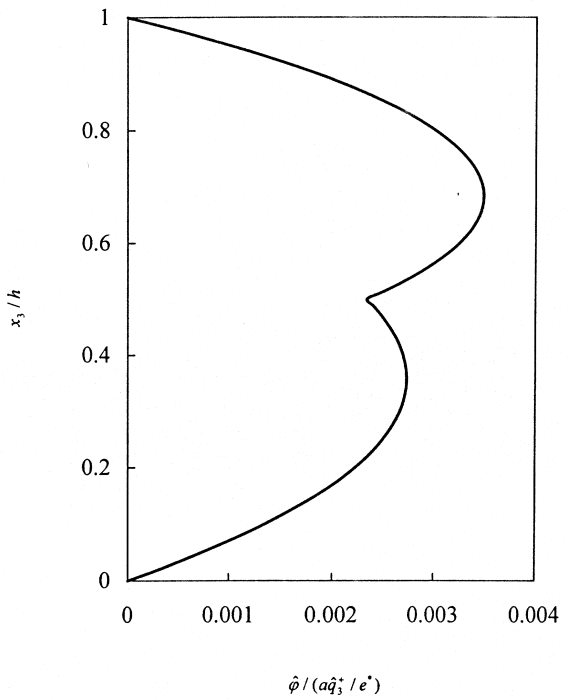

Fig. 1. Amplitude distribution of dimensionless electric potential through the thickness for a two-layer PZT-4/PVDF laminate under applied load ($a/b = 2$ and $a/h = 10$).

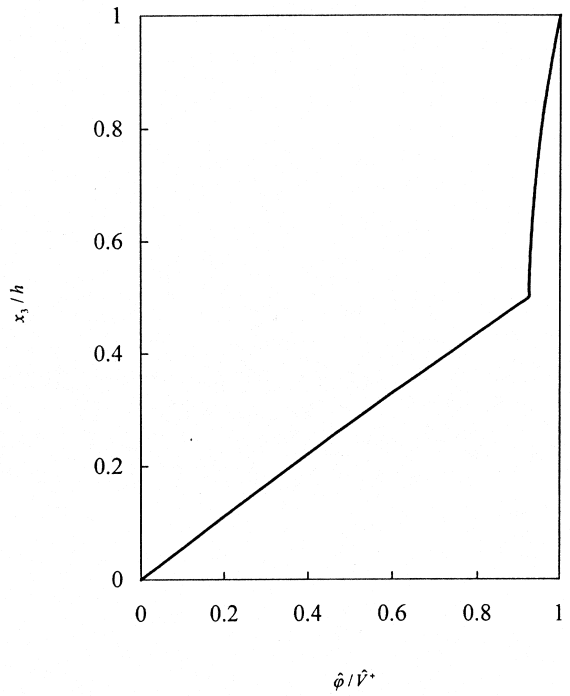

Fig. 2. Amplitude distribution of dimensionless electric potential through the thickness for a two-layer PZT-4/PVDF laminate under applied potential ($a/b = 2$ and $a/h = 10$).

Table 3
Amplitude of inplane mechanical displacement $\bar{u}_1 \times 10^{10}$ for a three-layer (0°/90°/0°) PVDF laminate ($a/b = 0$)

x_3/h	Applied load				Applied potential			
	$a/h = 4$	$a/h = 10$	$a/h = 20$	$a/h = 100$	$a/h = 4$	$a/h = 10$	$a/h = 20$	$a/h = 100$
1	−0.23887	−0.96691	−3.4965	−84.305	0.000740	−0.011595	−0.028813	−0.15374
0.9	−0.11750	−0.68979	−2.7113	−67.357	−0.004109	−0.014142	−0.030148	−0.15401
0.8	−0.03897	−0.44992	−1.9623	−50.446	−0.008397	−0.016753	−0.031546	−0.15430
0.7	0.02383	−0.23446	−1.2395	−33.561	−0.013679	−0.019574	−0.033026	−0.15460
2/3	0.04504	−0.16604	−1.0027	−27.937	−0.015966	−0.020587	−0.033541	−0.15470
0.6	0.02990	−0.09803	−0.6003	−16.761	−0.014161	−0.019620	−0.033032	−0.15460
0.5	0.00693	0.00293	0.0022	0.002	−0.010722	−0.017748	−0.032046	−0.15440
0.4	−0.01732	0.10364	0.6045	16.764	−0.006238	−0.015356	−0.030790	−0.15414
1/3	−0.03479	0.17120	1.0069	27.940	−0.002546	−0.013461	−0.029801	−0.15394
0.3	−0.01479	0.23939	1.2436	33.564	−0.003075	−0.013678	−0.029910	−0.15397
0.2	0.04435	0.45403	1.9662	50.449	−0.004362	−0.014377	−0.030278	−0.15404
0.1	0.11825	0.69286	2.7149	67.361	−0.005547	−0.015177	−0.030714	−0.15413
0	0.23239	0.96867	3.4998	84.309	−0.007054	−0.016124	−0.031224	−0.15423

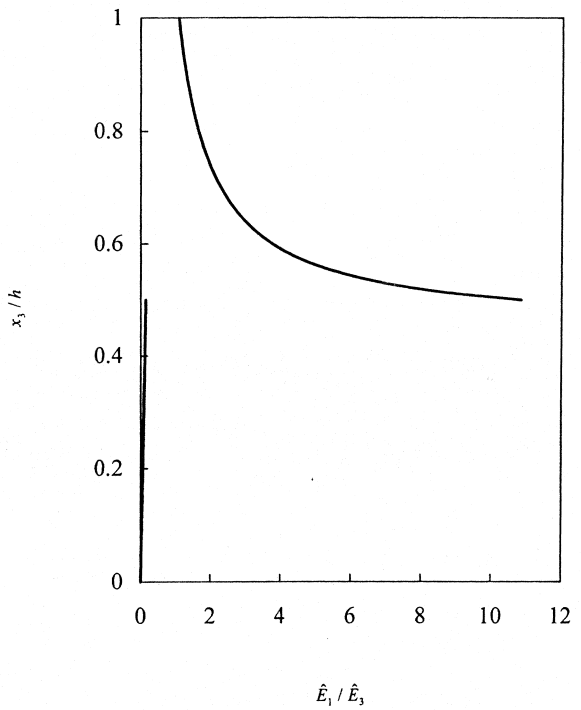

Fig. 3. Amplitude distribution of electric field components ratio through the thickness for a two-layer PZT-4/PVDF laminate under applied potential ($a/b = 2$ and $a/h = 10$).

Table 4
Amplitude of out-of-plane mechanical displacement $\bar{u}_3 \times 10^{10}$ for a three-layer (0°/90°/0°) PVDF laminate ($a/b = 0$)

x_3/h	Applied load				Applied potential			
	$a/h = 4$	$a/h = 10$	$a/h = 20$	$a/h = 100$	$a/h = 4$	$a/h = 10$	$a/h = 20$	$a/h = 100$
1	1.9716	9.5648	51.356	5401.2	0.23461	0.22532	0.22347	0.22280
0.9	1.9516	9.5614	51.362	5401.3	0.20436	0.19874	0.19744	0.19696
0.8	1.9318	9.5567	51.366	5401.3	0.17560	0.17241	0.17147	0.17112
0.7	1.9136	9.5514	51.368	5401.4	0.14817	0.14631	0.14556	0.14528
2/3	1.9079	9.5495	51.368	5401.4	0.13931	0.13766	0.13694	0.13667
0.6	1.8974	9.5459	51.368	5401.4	0.12191	0.12042	0.11970	0.11944
0.5	1.8841	9.5409	51.366	5401.4	0.09654	0.09466	0.09388	0.09361
0.4	1.8738	9.5365	51.363	5401.4	0.07183	0.06901	0.06808	0.06776
1/3	1.8686	9.5338	51.360	5401.4	0.05564	0.05196	0.05090	0.05053
0.3	1.8664	9.5325	51.359	5401.4	0.04760	0.04344	0.04231	0.04191
0.2	1.8612	9.5284	51.352	5401.3	0.02376	0.01794	0.01655	0.01607
0.1	1.8575	9.5236	51.344	5401.3	0.00019	−0.00752	−0.00919	−0.00976
0	1.8541	9.5177	51.333	5401.2	−0.02324	−0.03295	−0.03493	−0.03560

Table 5
Amplitude of out-of-plane shear stress $\bar{\tau}_{13}$ for a three-layer (0°/90°/0°) PVDF laminate ($a/b = 0$)

x_3/h	Applied load				Applied potential			
	$a/h = 4$	$a/h = 10$	$a/h = 20$	$a/h = 100$	$a/h = 4$	$a/h = 10$	$a/h = 20$	$a/h = 100$
1	0	0	0	0	0	0	0	0
0.9	1.0324	1.9422	3.6422	17.800	−0.016280	0.006570	0.011434	0.013112
0.8	1.4928	3.2800	6.3849	31.626	−0.005226	0.019371	0.024520	0.026292
0.7	1.5480	4.0850	8.2645	41.486	0.034232	0.038696	0.039337	0.039542
2/3	1.4847	4.2433	8.7039	43.892	0.055241	0.046689	0.044678	0.043975
0.6	1.4766	4.2662	8.7667	44.236	0.040759	0.029769	0.027274	0.026404
0.5	1.4739	4.2804	8.8028	44.429	0.018308	0.004197	0.001115	0.000045
0.4	1.4830	4.2705	8.7691	44.236	−0.005631	−0.021730	−0.025140	−0.026317
1/3	1.4960	4.2506	8.7078	43.893	−0.022809	−0.039282	−0.042712	−0.043895
0.3	1.5458	4.0905	8.2679	41.487	−0.024493	−0.036253	−0.038680	−0.039515
0.2	1.4643	3.2813	6.3868	31.627	−0.023832	−0.026060	−0.026297	−0.026364
0.1	1.0012	1.9415	3.6430	17.800	−0.015831	−0.014063	−0.013429	−0.013194
0	0	0	0	0	0	0	0	0

$x_3 = h$ (top) and the laminate interfaces are located at $x_3 = h/3$ and $2h/3$. For the discontinuous interfacial quantities, values at both neighboring surfaces of the interfaces are tabulated.

The mechanical inplane displacement $\bar{u}_1$, in the case of applied potential, is approximately constant through the thickness for a very thin plate (column 9 in Table 3) but it varies considerably in the case of applied load even if the plate is very thin (column 5 in Table 3). From the distributions of $\bar{u}_1$ in Table 3 and $\bar{\tau}_{13}$ in Table 5, the piezoelectric plate under applied load behaves similarly to a purely elastic plate. In particular, $\bar{u}_1$ is linear for a thin laminate and zigzag for a thick laminate (Pagano, 1969). Compared with the results of Heyliger and Brooks (1996) using $e_{113} = -0.01$, the through-thickness distributions of $\bar{u}_1$ and $\bar{\tau}_{13}$ are very sensitive to variation in e_{113} for a thick PVDF laminate under applied potential (column 6 in Tables 3 and 5), but it is rather indifferent to e_{113} when the laminate is thin (column 9 in

Table 6
Amplitude of out-of-plane normal stress $\bar{\tau}_{33}$ for a three-layer (0°/90°/0°) PVDF laminate ($a/b = 0$)

x_3/h	Applied load				Applied potential			
	$a/h = 4$	$a/h = 10$	$a/h = 20$	$a/h = 100$	$a/h = 4$	$a/h = 10$	$a/h = 20$	$a/h = 100$
1	1	1	1	1	0	0	0	0
0.9	0.95480	0.96777	0.97018	0.97098	0.0008329	−0.0000870	−0.0000877	−0.00002058
0.8	0.85263	0.88427	0.89028	0.89231	0.0018490	−0.0004779	−0.0003678	−0.00008246
0.7	0.73081	0.76726	0.77411	0.77642	0.0009183	−0.0013723	−0.0008671	−0.00018585
2/3	0.69102	0.72360	0.72965	0.73168	−0.0002430	−0.0018187	−0.0010869	−0.00022958
0.6	0.61352	0.63447	0.63814	0.63937	−0.0027574	−0.0026195	−0.0014637	−0.00030328
0.5	0.49771	0.50017	0.50007	0.50000	−0.0050843	−0.0031537	−0.0016867	−0.00034483
0.4	0.38167	0.36579	0.36197	0.36063	−0.0055943	−0.0028794	−0.0014982	−0.00030356
1/3	0.30371	0.27654	0.27043	0.26831	−0.0048548	−0.0022409	−0.0011430	−0.00023004
0.3	0.26381	0.23281	0.22595	0.22357	−0.0042332	−0.0018453	−0.0009299	−0.00018636
0.2	0.14333	0.11570	0.10974	0.10768	−0.0022840	−0.0008620	−0.0004190	−0.00008287
0.1	0.04368	0.03219	0.02982	0.02900	−0.0006797	−0.0002267	−0.0001063	−0.00002073
0	0	0	0	0	0	0	0	0

Table 7
Amplitude of electric potential $\bar{\varphi}$ for a three-layer (0°/90°/0°) PVDF laminate ($a/b = 0$)

x_3/h	Applied load				Applied potential			
	$a/h = 4$	$a/h = 10$	$a/h = 20$	$a/h = 100$	$a/h = 4$	$a/h = 10$	$a/h = 20$	$a/h = 100$
1	0	0	0	0	1	1	1	1
0.9	0.0014445	0.0019806	0.0033090	0.015431	0.88329	0.89735	0.89942	0.90011
0.8	0.0024851	0.0034655	0.0058526	0.027427	0.77211	0.79545	0.79893	0.80006
0.7	0.0033122	0.0045361	0.0076720	0.035995	0.66578	0.69437	0.69864	0.70007
2/3	0.0035504	0.0048103	0.0081228	0.038091	0.63130	0.66083	0.66525	0.66675
0.6	0.0038747	0.0052708	0.0089457	0.042050	0.56365	0.59397	0.59852	0.60004
0.5	0.0040411	0.0055279	0.0094081	0.044276	0.46479	0.49411	0.49854	0.50000
0.4	0.0038296	0.0052657	0.0089445	0.042050	0.36859	0.39471	0.39868	0.39996
1/3	0.0034823	0.0048024	0.0081208	0.038091	0.30566	0.32865	0.33215	0.33332
0.3	0.0032413	0.0045280	0.0076701	0.035995	0.27449	0.29568	0.29891	0.29998
0.2	0.0024171	0.0034581	0.0058510	0.027426	0.18204	0.19696	0.19924	0.19998
0.1	0.0013971	0.0019757	0.0033081	0.015431	0.09073	0.09843	0.09961	0.09999
0	0	0	0	0	0	0	0	0

Tables 3 and 5). In other words, the solutions of thick laminates under applied potential differ significantly from the solutions of Heyliger and Brooks (1996) while the thin laminate solutions do not. Note that for a laminate under applied load, the transverse mechanical displacement $\bar{u}_3$ is approximately constant through the thickness even for a thick plate with $a/h = 4$ (columns 2–5 in Table 4). By contrast, in the case of applied potential, its distribution is not constant (columns 6–9 in Table 4). Therefore, assuming at least a piecewise linear distribution along the thickness direction for $\bar{u}_3$ is necessary in this case for constructing a proper two-dimensional approximate theory.

The distribution of electric potential is presented in Table 7. For both thin and thick laminates, its distribution is approximately piecewise parabolic for applied load while it is approximately piecewise linear for applied potential. It is noted that the transverse electric displacement $\bar{D}_3$ varies insignificantly

Table 8
Amplitude of transverse electrical displacement $\bar{D}_3 \times 10^{10}$ for a three-layer (0°/90°/0°) PVDF laminate ($a/b = 0$)

x_3/h	Applied load				Applied potential			
	$a/h = 4$	$a/h = 10$	$a/h = 20$	$a/h = 100$	$a/h = 4$	$a/h = 10$	$a/h = 20$	$a/h = 100$
1	−0.23462	−0.22531	−0.22345	−0.22282	−5.4216	−11.695	−22.839	−113.31
0.9	−0.22054	−0.21531	−0.21421	−0.21383	−5.1552	−11.588	−22.785	−113.30
0.8	−0.18863	−0.18937	−0.18943	−0.18944	−4.9211	−11.492	−22.737	−113.29
0.7	−0.15042	−0.15301	−0.15340	−0.15352	−4.7173	−11.407	−22.695	−113.28
2/3	−0.13789	−0.13944	−0.13961	−0.13966	−4.6557	−11.381	−22.682	−113.28
0.6	−0.13400	−0.13536	−0.13548	−0.13551	−4.5513	−11.338	−22.660	−113.27
0.5	−0.12811	−0.12916	−0.12921	−0.12922	−4.4166	−11.281	−22.631	−113.27
0.4	−0.12221	−0.12297	−0.12295	−0.12293	−4.3076	−11.234	−22.607	−113.26
1/3	−0.11831	−0.11888	−0.11881	−0.11879	−4.2488	−11.209	−22.595	−113.26
0.3	−0.10575	−0.10529	−0.10502	−0.10492	−4.2216	−11.197	−22.589	−113.26
0.2	−0.06798	−0.06890	−0.06898	−0.06900	−4.1575	−11.169	−22.575	−113.26
0.1	−0.03686	−0.04297	−0.04419	−0.04461	−4.1194	−11.153	−22.566	−113.25
0	−0.02325	−0.03297	−0.03495	−0.03562	−4.1068	−11.147	−22.564	−113.25

Table 9
Amplitude of inplane stress $\bar{\tau}_{11}$ for a three-layer (0°/90°/0°) PVDF laminate ($a/b = 0$)

x_3/h	Applied load				Applied potential			
	$a/h = 4$	$a/h = 10$	$a/h = 20$	$a/h = 10$	$a/h = 4$	$a/h = 10$	$a/h = 20$	$a/h = 10$
1	18.055	72.454	261.46	6299.4	−0.40572	0.11042	0.6766	4.1633
0.9	8.978	51.742	202.79	5033.0	−0.02602	0.30764	0.7798	4.1843
0.8	3.089	33.802	146.81	3769.4	0.30970	0.50886	0.8873	4.2063
0.7	−1.628	17.679	92.78	2507.8	0.71739	0.72489	1.0005	4.2293
2/3	−3.220	12.558	75.08	2087.5	0.89194	0.80215	1.0398	4.2372
2/3	−0.202	1.352	7.49	204.9	−0.27442	−0.80629	−1.6612	−8.3893
0.6	−0.106	0.836	4.52	123.0	−0.27939	−0.80986	−1.6632	−8.3897
0.5	0.039	0.069	0.07	0.1	−0.29374	−0.81890	−1.6680	−8.3907
0.4	0.194	−0.696	−4.37	−122.8	−0.31754	−0.83247	−1.6752	−8.3922
1/3	0.306	−1.209	−7.34	−204.8	−0.33952	−0.84411	−1.6813	−8.3934
1/3	2.659	−12.738	−75.18	−2087.6	−0.08549	0.28076	0.7659	4.1815
0.3	1.157	−17.842	−92.88	−2507.8	−0.04407	0.29784	0.7745	4.1832
0.2	−3.287	−33.903	−146.89	−3769.5	0.05669	0.35206	0.8030	4.1890
0.1	−8.828	−51.765	−202.85	−5033.1	0.14806	0.41308	0.8362	4.1958
0	−17.365	−72.380	−261.50	−6299.4	0.26160	0.48419	0.8745	4.2037

for applied potential for not very thick PVDF laminates (columns 7–9 in Table 8) as $\bar{D}_3$ is almost constant through the thickness. However, $\bar{D}_3$ varies significantly for applied load, even if for a thin plate (columns 2–5 in Table 8).

5. Conclusions

An asymptotic scheme for anisotropic inhomogeneous and laminated piezoelectric plates in the

Table 10
Amplitude of inplane stress $\bar{\tau}_{22}$ for a three-layer (0°/90°/0°) PVDF laminate ($a/b = 0$)

x_3/h	Applied load				Applied potential			
	$a/h = 4$	$a/h = 10$	$a/h = 20$	$a/h = 100$	$a/h = 4$	$a/h = 10$	$a/h = 20$	$a/h = 100$
1	0.45617	1.2909	4.1888	96.758	−0.45664	−0.96995	−1.8871	−9.3498
0.9	0.30918	0.9678	3.2841	77.339	−0.42852	−0.95801	−1.8811	−9.3486
0.8	0.20123	0.6783	2.4120	57.952	−0.40373	−0.94703	−1.8755	−9.3475
0.7	0.10787	0.4109	1.5636	38.589	−0.38073	−0.93686	−1.8703	−9.3464
2/3	0.07658	0.3248	1.2845	32.139	−0.37317	−0.93362	−1.8687	−9.3461
2/3	0.09331	0.3423	1.3021	32.156	−0.28270	−0.71249	−1.4279	−7.1449
0.6	0.09365	0.2448	0.8209	19.334	−0.27858	−0.71095	−1.4272	−7.1447
0.5	0.09456	0.0996	0.1005	0.101	−0.27433	−0.70953	−1.4265	−7.1446
0.4	0.09690	−0.0452	−0.6199	−19.132	−0.27253	−0.70920	−1.4264	−7.1446
1/3	0.09981	−0.1422	−1.1009	−31.955	−0.27280	−0.70960	−1.4266	−7.1446
1/3	0.09133	−0.1502	−1.1087	−31.962	−0.35526	−0.92736	−1.8656	−9.3455
0.3	0.06141	−0.2360	−1.3877	−38.413	−0.35224	−0.92605	−1.8650	−9.3454
0.2	−0.02753	−0.5025	−2.2359	−57.775	−0.34499	−0.92273	−1.8633	−9.3450
0.1	−0.12972	−0.7908	−3.1077	−77.162	−0.34010	−0.92030	−1.8620	−9.3448
0	−0.26816	−1.1124	−4.0120	−96.581	−0.33718	−0.91870	−1.8612	−9.3446

Table 11
Amplitude of inplane electrical displacement $\bar{D}_1 \times 10^{10}$ for a three-layer (0°/90°/0°) PVDF laminate ($a/b = 0$)

x_3/h	Applied load				Applied potential			
	$a/h = 4$	$a/h = 10$	$a/h = 20$	$a/h = 100$	$a/h = 4$	$a/h = 10$	$a/h = 20$	$a/h = 100$
1	0	0	0	0	−3.6072	−3.6072	−3.6072	−3.6072
0.9	−0.32196	−0.6030	−1.1294	−5.517	−3.1812	−3.2389	−3.2479	−3.2509
0.8	−0.46698	−1.0189	−1.9801	−9.802	−2.7835	−2.8753	−2.8894	−2.8940
0.7	−0.48689	−1.2697	−2.5634	−12.859	−2.4121	−2.5166	−2.5322	−2.5374
2/3	−0.46833	−1.3193	−2.6998	−13.604	−2.2942	−2.3980	−2.4134	−2.4185
2/3	−0.07398	−0.1937	−0.3914	−1.964	−2.1068	−2.2049	−2.2195	−2.2245
0.6	−0.07473	−0.1962	−0.3968	−1.992	−1.8807	−1.9813	−1.9964	−2.0014
0.5	−0.07517	−0.1976	−0.3999	−2.007	−1.5502	−1.6473	−1.6620	−1.6668
0.4	−0.07484	−0.1963	−0.3969	−1.992	−1.2285	−1.3149	−1.3280	−1.3322
1/3	−0.07423	−0.1939	−0.3916	−1.964	−1.0180	−1.0939	−1.1055	−1.1093
1/3	−0.47157	−1.3215	−2.7010	−13.605	−1.0956	−1.1735	−1.1850	−1.1889
0.3	−0.48598	−1.2714	−2.5644	−12.859	−0.9826	−1.0554	−1.0663	−1.0700
0.2	−0.45798	−1.0192	−1.9807	−9.803	−0.6493	−0.7025	−0.7106	−0.7133
0.1	−0.31221	−0.6028	−1.1297	−5.517	−0.3224	−0.3507	−0.3552	−0.3566
0	0	0	0	0	0	0	0	0

framework of three-dimensional piezoelectricity has been presented. Without accounting for boundary layer effects, an interior solution can be obtained using a numerical recurrence procedure to the desired accuracy.

Numerical examples presented have shown excellent agreement with published data. In addition, new results for two different piezoelectric laminates comprised of PZT-4 and PVDF materials have been presented. Significant physical interpretations have been discussed. The two-dimensional piezoelectric plate models that make certain assumptions through the laminate thickness, such as linear electric potential for applied load or constant transverse displacement for applied potential, is not consistent with the results presented in this paper even for a thin plate. In addition, neglect of the inplane electric field is questionable at least in the case where the top and bottom transverse electric displacements are unequal.

In contrast to almost all approximate two-dimensional plate theories which provide no insight into the significance of neglecting certain physical quantities, the asymptotic approach developed here is able not only to obtain accurate interior solutions and important physical insights but also to assess the order of error involved.

Acknowledgements

Partial financial support from the National Natural Science Foundation of China is gratefully acknowledged by the first author.

References

Batra, R.C., Liang, X.Q., Yang, J.S., 1996a. Shape control of vibrating simply supported rectangular plates. AIAA J. 34, 116–122.
Batra, R.C., Liang, X.Q., Yang, J.S., 1996b. The vibration of a simply supported rectangular elastic plates due to piezoelectric actuators. Int. J. Solids Struct. 33, 1597–1618.

Berlincourt, D.A., Curran, D.R., Jaffe, H., 1964. Piezoelectric and piezomagnetic materials and their function in transducers. In: Mason, W.P. (Ed.), Physical Acoustics, vol. 1. Academic Press, New York, pp. 169–270.

Bisegna, P., Maceri, F., 1996a. An exact three-dimensional solution for simply supported rectangular piezoelectric plates. J. Appl. Mech. 63, 628–638.

Bisegna, P., Maceri, F., 1996b. A consistent theory of thin piezoelectric plates. J. Intell. Mater. Syst. Struct. 7, 372–389.

Cheng, Z.Q., Lim, C.W., Kitipornchai, S., 1999. Three-dimensional exact solution for inhomogeneous and laminated piezoelectric plates. Int. J. Engng Sci. 37, 1425–1439.

Crawley, E.F., de Luis, J., 1987. Use of piezoelectric actuators as elements of intelligent structures. AIAA J. 25, 1373–1385.

Gol'denveizer, A.L., 1969. Boundary layer and its interaction with the interior state of stress of an elastic thin shell. J. Appl. Math. Mech. 33, 971–1001.

Heyliger, P., 1994. Static behavior of laminated elastic/piezoelectric plates. AIAA J. 32, 2481–2484.

Heyliger, P., 1997. Exact solutions for simply supported laminated piezoelectric plates. J. Appl. Mech. 64, 299–306.

Heyliger, P., Brooks, S., 1996. Exact solutions for laminated piezoelectric plates in cylindrical bending. J. Appl. Mech. 63, 903–910.

Heyliger, P., Pei, K.C., Saravanos, D., 1996. Layerwise mechanics and finite element model for laminated piezoelectric shells. AIAA J. 34, 2353–2360.

Huang, J.H., Wu, T.L., 1996. Analysis of hybrid multilayered piezoelectric plates. Int. J. Engng Sci. 34, 171–181.

Koconis, D.B., Kollár, L.P., Springer, G.S., 1994a. Shape control of composite plates and shells with embedded actuators. I. Voltages specified. J. Compos. Mater. 28, 415–458.

Koconis, D.B., Kollár, L.P., Springer, G.S., 1994b. Shape control of composite plates and shells with embedded actuators. II. Desired shape specified. J. Compos. Mater. 28, 459–482.

Lee, C.K., 1990. Theory of laminated piezoelectric plates for the design of distributed sensors/actuators. Part I: Governing equations and reciprocal relationships. J. Acoust. Soc. Am. 87, 1144–1158.

Lee, C.K., Moon, F.C., 1989. Laminated piezopolymer plates for torsion and bending sensors and actuators. J. Acoust. Soc. Am. 85, 2432–2439.

Lee, J.S., Jiang, L.Z., 1996. Exact electroelastic analysis of piezoelectric laminae via state space approach. Int. J. Solids Struct. 33, 977–990.

Librescu, L., Meirovitch, L., Na, S.S., 1997. Control of cantilever vibration via structural tailoring and adaptive materials. AIAA J. 35, 1309–1315.

Librescu, L., Meirovitch, L., Song, O., 1996. Integrated structural tailoring and adaptive materials control for advanced aircraft wings. J. Aircraft 33, 203–213.

Librescu, L., Song, O., Rogers, C.A., 1993. Adaptive vibrational behavior of cantilevered structures modeled as composite thin-walled beams. Int. J. Engng Sci. 31, 775–792.

Mason, W.P., 1981. Piezoelectricity, its history and applications. J. Acoust. Soc. Am. 70, 1561–1566.

Maugin, G.A., 1988. Continuum Mechanics of Electromagnetic Solids. North-Holland, Amsterdam.

Maugin, G.A., Attou, D., 1990. An asymptotic theory of thin piezoelectric plates. Q. J. Mech. Appl. Math. 43, 347–362.

Mindlin, R.D., 1972. High frequency vibrations of piezoelectric crystal plates. Int. J. Solids Struct. 8, 895–906.

Mitchell, J.A., Reddy, J.N., 1995. A refined hybrid plate theory for composite laminates with piezoelectric laminae. Int. J. Solids Struct. 32, 2345–2367.

Pagano, N.J., 1969. Exact solutions for composite laminates in cylindrical bending. J. Compos. Mater. 3, 398–411.

Pagano, N.J., 1970. Exact solutions for rectangular bi-directional composites and sandwich plates. J. Compos. Mater. 4, 20–34.

Reddy, J.N., 1997. Mechanics of Laminated Composite Plates: Theory and Analysis. CRC Press, Boca Raton, Florida.

Reddy, J.N., 1999. On laminated composite plates with integrated sensors and actuators. Engng Struct. 21, 568–593.

Sosa, H.A., 1992. On the modelling of piezoelectric laminated structures. Mech. Res. Commun. 19, 541–546.

Tarn, J.Q., 1994. An asymptotic theory for dynamic response of anisotropic inhomogeneous and laminated cylindrical shells. J. Mech. Phys. Solids 42, 1633–1650.

Tarn, J.Q., 1996a. Elastic buckling of multilayered anisotropic plates. J. Mech. Phys. Solids 44, 389–411.

Tarn, J.Q., 1996b. An asymptotic variational formulation for dynamic analysis of multilayered anisotropic plates. Comput. Methods Appl. Mech. Engng 130, 337–353.

Tarn, J.Q., Wang, Y.M., 1994. An asymptotic theory for dynamic response of anisotropic inhomogeneous and laminated plates. Int. J. Solids Struct. 31, 231–246.

Tarn, J.Q., Wang, Y.M., 1995. Asymptotic thermoelastic analysis of anisotropic inhomogeneous and laminated plates. J. Thermal Stresses 18, 35–58.

Tarn, J.Q., Wang, Y.B., 1997. A refined asymptotic theory and computational model for multilayered composite plates. Comput. Methods Appl. Mech. Engng. 145, 167–184.

Tarn, J.Q., Yen, C.B., 1995. A three-dimensional asymptotic analysis of anisotropic inhomogeneous and laminated shells. Acta Mech. 113, 137–153.

Tashiro, K., Tadokoro, H., Kobayashi, M., 1981. Structure and piezoelectricity of poly (vinylidene fluoride). Ferroelectrics 32, 167–175.

Tauchert, T.R., 1992. Piezothermoelastic behavior of a laminated plate. J. Thermal Stresses 15, 25–37.

Tiersten, H.F., 1969. Linear Piezoelectric Plate Vibrations. Plenum Press, New York.

Tzou, H.S., 1993. Piezoelectric Shells: Distributed Sensing and Control of Continua. Kluwer Academic Publishers, Dordrecht.

Tzou, H.S., Bao, Y., 1995. A theory on anisotropic piezothermoelastic shell laminates with sensor/actuators applications. J. Sound Vib. 184, 453–473.

Wang, B.T., Rogers, C.A., 1991. Laminated theory for spatially distributed induced strain actuators. J. Compos. Mater. 25, 433–453.

Wang, Y.M., Tarn, J.Q., 1994. A three-dimensional analysis of anisotropic inhomogeneous and laminated plates. Int. J. Solids Struct. 31, 497–515.

Whitney, J.M., 1987. Structural Analysis of Laminated Anisotropic Plates. Technomic Publishing, Lancaster.

Wu, C.P., Tarn, J.Q., Chi, S.M., 1996a. Three-dimensional analysis of doubly curved laminated shells. J. Engng. Mech. 122, 391–401.

Wu, C.P., Tarn, J.Q., Chi, S.M., 1996b. An asymptotic theory for dynamic response of doubly curved laminated shells. Int. J. Solids Struct. 33, 3813–3841.

Wu, C.P., Tarn, J.Q., Yang, K.L., 1996c. Thermoelastic analysis of doubly curved laminated shells. J. Thermal Stresses 19, 531–563.

Xu, K., Noor, A.K., Tang, Y.Y., 1995. Three-dimensional solutions for coupled thermoelectroelastic response of multilayered plates. Comput. Methods Appl. Mech. Engng. 126, 355–371.

Xu, K., Noor, A.K., Tang, Y.Y., 1997. Three-dimensional solutions for free vibrations of initially-stressed thermoelectroelastic multilayered plates. Comput. Methods Appl. Mech. Engng. 141, 125–139.

Zhou, Y.S., Tiersten, H.F., 1994. Elastic analysis of laminated composite plates in cylindrical bending due to piezoelectric actuators. Smart Mater. Struct. 3, 255–265.